Efficient synthesis of 2,5-dihydroxymethylfuran and 2,5-dimethylfuran from 5-hydroxymethylfurfural using minerals-derived Cu catalysts as versatile catalysts

Yifeng Zhu,[a,b,‡] Xiao Kong,[a,b,‡] Hongyan Zheng,[c] Guoqiang Ding,[c] Yulei Zhu,*[a,c] and Yong-Wang Li[a,c]

Table of contents

Minerals-derived Cu/ZnO as a versatile catalyst.

Cu/ZnO catalyst derived from minerals (malachite, rosasite and aurichalcite) could catalyze 5-hydroxymethylfurfural hydrogenation to 2,5-dihydroxymethylfuran and 2,5-dimethylfuran tunably.

Catalysis Science & Technology

ARTICLE TYPE

Efficient synthesis of 2,5-dihydroxymethylfuran and 2,5-dimethylfuran from 5-hydroxymethylfurfural using minerals-derived Cu catalysts as versatile catalysts

Yifeng Zhu,[a,b,‡] Xiao Kong,[a,b,‡] Hongyan Zheng,[c] Guoqiang Ding,[c] Yulei Zhu,*[a,c] and Yong-Wang Li[a,c]

Selective conversion of 5-hydroxymethylfurfural (HMF) can produce sustainable fuels and chemicals. Herein, Cu-ZnO catalysts derived from the minerals (malachite, rosasite and aurichalcite) were employed for selective hydrogenation of HMF for the first time. High yields of 2,5-dihydroxymethylfuran (~99.1%) 10 and 2,5-dimethylfuran (~91.8%) were obtained tunably over the catalyst with Cu/Zn molar ratio of 2, due to the well-dispersed metal sites by tailored mineral precursors, well-controlled surface sites and optimized reaction conditions. The relationship between catalytic performance and catalyst properties were elucidated by characterizations on composition, structural and surface properties and catalytic tests. The catalyst can also be extended to selective hydrogenation of other bio-derived molecules (furfural and 15 5-methylfurfural) to targeted products. The construction of minerals-derived Cu-ZnO catalysts and revelation of structure-performance relationship can be applied to the further rational design and functionalization of non-noble Cu catalysts for selective conversion of bio-derived compounds.

Introduction

Growing interests have been paid on utilization of renewable 20 biomass to substitute the shrinking fossil resources for energy and chemical supply. 5-hydroxymethylfurfural (HMF) is an important platform chemical which could be facilely obtained from renewable biomass resources (e.g., cellulose, glucose and fructose) using acid catalysts.[1, 2] It contains many functional 25 groups including C=O, C-O, C=C and furan ring, which allow it to be hydrogenated into various products (e.g., 2,5-dihydroxymethylfuran (DHMF), 2,5-dimethylfuran (DMF), 2,5-dihydroxymethyltetrahydrofuran (DHMTHF) and 2,5-dimethyltetrahydrofuran (DMTHF)).[1] Among the derivatives, 30 DHMF and DMF attract great interests. In this paper, we are aiming at tunable synthesis of DHMF and DMF over the same non-noble catalyst, which is a challenging but valuable work for both academic and industrial purposes.

DHMF is a promising diol, which could be either directly used 35 for producing shape memory and self-healing polymers, or used for synthesis of 1,6-hexanediol which is also an important polymer precursor.[3-5] Besides, it can also be employed for production of intermediates of drugs and crown ethers.[6] Selective hydrogenation of HMF to DHMF is a reaction of hydrogenation 40 of aldehyde group. The side reactions involving of C=C, C-O and furan-ring hydrogenation should be suppressed.

DMF is an alternative fuel with high energy density (30 kJ/cm³) and octane number (RON=119), holding great potential to

substitute the petroleum-based gasolines.[7] As a diene, DMF can 45 also be converted to valuable benzene-chemicals via Diels-Alder reactions.[8, 9] Production of DMF from HMF is a reaction involving of C=O hydrogenation and C-O hydrogenolysis, while the C=C hydrogenation and ring-opening reactions need to be avoided.

50 Previous works on selective hydrogenation of HMF to DHMF and DMF were mainly performed on noble metal catalysts, which is a great impediment for the industrial applications. For DHMF synthesis, Alamillo et al.[10] studied the supported Ru, Pd and Pt catalysts for HMF hydrogenation, of which Ru was the most 55 active metal with a yield of 81%-94%. Au/Al₂O₃ catalyst was proposed for DHMF production with 96% yield at 140 °C and 3.8 MPa.[11] Other catalysts were also reported, including Pt/MCM-41[6], Pd/C[12] and Ir-ReOₓ/SiO₂[13]. For DMF production, Dumesic et al.[7] reported for the first time a Ru-Cu catalyst with a yield of 60 76~79%. Many following reports were also mainly conducted on noble metals (e.g., Pd[12], Ru[14, 15] and Pt[16]). However, few reports existed on development of non-noble substitutes, due to the low reactivity. Ni-based (e.g., Raney Ni[17], Ni/Al₂O₃[18] and Ni-W₂C/AC[19]) catalysts were emerging for DMF synthesis, while 65 they were difficult to be employed in DHMF synthesis, due to the strong C=C hydrogenation ability of Ni. Recently, the Cu/MgO/Al₂O₃ and Ru-modified Cu/MgO/Al₂O₃ catalysts derived from hydrotalcite were employed in synthesis of DHMF and DMF.[20, 21] Nevertheless, the development of non-noble 70 catalysts still requires considerable efforts prior to the commercial applications.

This journal is © The Royal Society of Chemistry [year]

Catal. Sci. Technol., [year], **[vol]**, 00–00 | **1**

Another challenge for HMF hydrogenation is the poor selectivity of products, due to the presence of many functional groups of HMF, DHMF and DMF. To obtain the high yields of DHMF/DMF, the efficiency for C=O hydrogenation and/or C-O hydrogenolysis need to be promoted. The commonly used noble metals (e.g., Ru, Pd) and Ni catalysts are good candidates, whereas the saturation of furan-ring is easily proceeded over these catalysts with strong C=C hydrogenation ability.[17, 18, 22] For example, DHMF yield would be reduced by the formation of DHMTHF over Raney Ni and Ni-Al$_2$O$_3$ catalysts.[17, 18] Ru-modified Cu/MgO/Al$_2$O$_3$ catalysts was reported for HMF hydrogenation with high reactivity.[20] However, Ru sites would also promote C=C hydrogenation reactions and lower the DMF yield. Control of surface acidity is also crucial. Proper amount of acid sites and high reaction temperature would facilitate the DMF formation via hydrogenolysis of CH$_2$OH groups, whereas CH$_2$OH groups need to be preserved for DHMF production.[20, 23] Besides, the excessive acid sites would catalyze the ring-opening reactions and etherification, and thus lower the selectivity of DHMF and DMF.[10] Thus, the choice of metal, proper surface acidity and reaction conditions are important for tunable synthesis of DHMF and DMF from HMF, in particular over the same catalyst. Cu catalyst is one of the best material for selective hydrogenations, due to the high reactivity for C=O and C-O bonds and relatively low reactivity for C=C and C-C bonds.[24-26] ZnO, as a catalyst support, has moderate surface acidity, facilitating the possibility for tunable synthesis of DHMF and DMF.
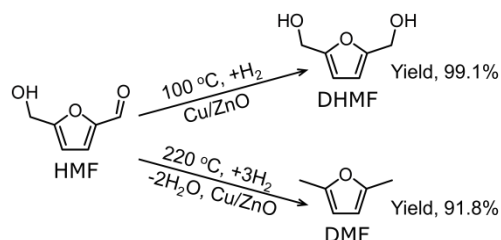
Scheme 1 Tunable synthesis of DHMF and DMF from HMF hydrogenation.

In view of the above problems, rational design of efficient non-noble catalyst based on the composition, structure and properties of materials is the prerequisite. Herein, we reported that the mineral-derived Cu-ZnO catalysts (malachite, rosasite and aurichalcite) can efficiently catalyze the selective conversion of HMF into either DHMF or DMF for the first time (**Scheme 1**). This work possesses at least the following desired features, 1) highly selective and tunable synthesis of DHMF and DMF over the non-noble Cu catalysts was realized; 2) the highly dispersed Cu sites and high reactivity of the catalysts can be achieved by using Cu-Zn binary minerals as precursors; 3) the revelation of structure-performance relationship can facilitate the further rational development of active Cu catalysts. Besides, the minerals-derived Cu-ZnO catalysts can be extended into selective conversion of other bio-derived molecules (furfural and 5-methylfurfural), demonstrating the great potential of catalysts in biomass utilizations.

Experimental Section

Preparation and evaluation

Copper nitrate trihydrate, zinc nitrate hexahydrate and sodium carbonate were purchased from Sinopharm. Co. Ltd. and used as received. The catalyst precursors were prepared by a facile constant pH co-precipitation method.[27] A solution containing copper nitrate and zinc nitrate with the preset Cu/Zn molar ratios was prepared. An aqueous solution of Na$_2$CO$_3$ (2 mol/L) was employed as precipitant. The two solutions were then simultaneously introduced into a 2 L vessel at 65 ^{o}C and a pH of 6.5±0.2. After precipitation, the suspension was aged for 150 min in the mother liquor and then washed and dried at 65 ^{o}C for 12 h, followed by calcination at 350 ^{o}C for 4 h in air. The resulted samples were denoted as CuZn-x, of which x indicates the molar ratio of Cu/Zn. As comparison, the catalyst without addition of Zn^{2+} was denoted as CuZn-inf, of which inf means infinite.

Prior to the tests, the catalyst was ex-situ reduced on a tube-reactor under H$_2$ atmosphere at 250 ^{o}C (heating rate of 0.5 ^{o}C/min) for 2 h. The tests were performed in an autoclave reactor (100 mL) after the ex-situ reduction of catalysts. Typically, 1.5 g HMF (Shanghai De-Mo Pharmaceutical Science and Technology Ltd. Co., 98%), 35 mL 1,4-dioxane (Sinopharm, A.R.) and 0.5 g catalyst were added into the reactor. The reactor was then sealed and purged by H$_2$ for 5 times. After that, the reactor was filled with H$_2$ in desired pressure and heated to objective temperature. After the tests, the products were collected and analyzed by a GC instrument with a FID detector.

Characterizations

The element compositions were determined by the inductively coupled plasma-optical emission spectroscopy (ICP, Perkin Elmer Optima 2100DV). XRD experiments were conducted on a Rigaku D/max-2000 diffractometer with Cu kα radiation operating at 40 kV. The BET surface areas, pore diameters and pore volumes of calcined catalysts were tested via N$_2$ physical adsorption at -196 ^{o}C using a Micrometritics ASAP 2420 instrument, after the samples were degassed at 90 ^{o}C for 1 h and 350 ^{o}C for 8 h. H$_2$ temperature-programmed reduction (TPR) and N$_2$O titration experiments were performed on a Tianjin XQ TP-5080 instrument equipped with a TCD detector. The surface acidity of catalysts was determined by temperature-programmed desorption of ammonia (NH$_3$-TPD) using a Micrometritics ASAP 2920 instrument and a mass spectrometric detector. The infrared (IR) spectra of the catalysts were obtained by a Nicolet NEXUS 470 FT-IR spectrometer in the range of 400-4000 cm^{-1} with a 4 cm^{-1} resolution. Raman spectra of the samples were recorded using a LabRAMHR800 system equipped with a CCD detector at room temperature. The 325 nm of the He–Cd laser was employed as the exciting source with a power of 30 MW. Thermo-gravity (TG) experiments of fresh reduced and used catalysts were performed on a Mettler Toledo TGA/SDTA 851 instrument (air atmosphere and heating rate of 10 ^{o}C/min). Prior to the test, both the fresh reduced and used catalysts were dried in air at 100 ^{o}C for 24 h.

Results and discussion

Brief introduction of the precursors

Malachite is the carbonate with a formula of [Cu$_2$(CO$_3$)(OH)$_2$]. It contains two crystallographically different CuO$_6$ octahedral sites which are coordinated by six O-atoms of CO$_3^{2-}$ and OH$^-$ ions in a

Jahn-Teller distorted octahedron.[28, 29] When some Zn^{2+} ions were added (Cu/Zn molar ratio > 2.7), single phase rosasite with a general formula of $[(Cu,Zn)_2(CO_3)(OH)_2]$ can be obtained.[30] Although it has similar composition to malachite, rosasite is not isomorphous with malachite. The main difference between them is the orientation of the Jahn-Teller elongated axes of CuO_6 octahedra.[31] Addition of higher amount of Zn^{2+} ions (Cu/Zn molar ratio < 2.7) results in the formation of aurichalcite which has a general formula of $[(Cu,Zn)_5(OH)_6(CO_3)_2]$.[29, 30] Aurichalcite contains four crystallographically different metal sites (Cu^{2+} and/or Zn^{2+}) in the lattice (denoted as M1, M2, M3 and M4), of which M1 and M2 are coordinated with six O-atoms; M3 is coordinated with four O-atoms and M4 is located at a fivefold trigonal bipyramid.[28, 29] M3 is totally occupied by Zn^{2+} while the others can be occupied by Cu^{2+} and Zn^{2+} with equal probability.[28, 32]
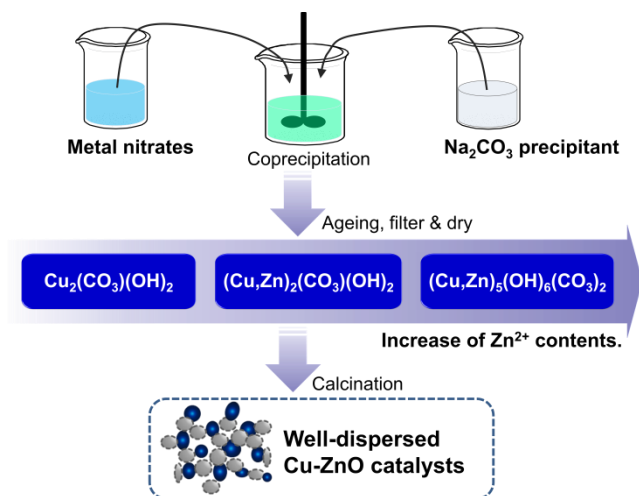
Scheme 2 Synthesis of Cu-ZnO catalysts with mineral precursors using a constant-pH coprecipitation method (pH value was adjusted by controlling the dropping speeds).

Despite of the different and complex formulas and structures, malachite, rosasite and aurichalcite minerals can be tunably synthesized simply through a constant pH coprecipitation method by varying the Cu/Zn molar ratios (**Scheme 2**).[27] Due to the homogeneous distributions of elements (Cu and Zn) in the minerals and different morphologies, these above minerals are important precursors for construction and meso-/nano-structuring of Cu-ZnO catalysts.[30] Herein, the above minerals were obtained at different preset Cu/Zn molar ratios (1, 2, 3, 4 and infinite). Upon calcination and reduction, highly dispersed Cu-ZnO catalysts with different Cu loadings were obtained and exhibited high performance for tunable production of DHMF (99.1%) and DMF (91.8%) from HMF hydrogenation.

Moreover, the contents of active phases and the compositions are highly flexible in a wide range for the mineral derived catalysts (e.g., the tunable Cu/Zn ratios and substitution of Cu^{2+}/Zn^{2+} by other divalent ions[33-35]), facilitating the further functionalization of catalysts. The present work demonstrated the design and construction of Cu-ZnO catalyst from some simple mineral precursors, which is a promising direction for catalyst design in selective hydrogenation of bio-derived molecules.

Characterizations of catalyst precursors

The different catalyst precursors were prepared via modulating the preset Cu/Zn molar ratios (CuZn-x, x indicates Cu/Zn ratios and inf means infinite). **Figure 1** shows XRD spectra of catalyst precursors in the range of 10-40°, which serves as the "fingerprint region" for identification of malachite, rosasite and aurichalcite minerals.[27, 29, 36] Evident peaks at 14.8° (020), 17.6° (120), 24.1° (220), 31.2° (20-1), 32.2° (21-1) and 35.6° (240) were observed for the CuZn-inf precursor, which can be assigned to characteristics of pure malachite (PDF#41-1390). Addition of little Zn^{2+} ions (CuZn-4 and CuZn-3) would lead to the structural change from malachite to rosasite. According to Behrens et al.[31], the (20-1) and (21-1) diffractions can be employed to distinguish the structural evolution because the cell volume shrinking would be proceeded when Cu-O bond is substituted by Zn-O bond. The peaks at 31.2° (20-1) and 32.2° (21-1) migrated toward higher angles (32.1° and 33.0°) while the peak intensity decreased, indicating the substitution of Cu^{2+} by Zn^{2+} in the lattice and the formation of rosasite crystalline. Further addition of Zn^{2+} (CuZn-2 and CuZn-1) resulted in the continuing decrease of peak intensity and emergence of peaks at 13.0° and 34.3°. The two emerged peaks belong to the characteristics of aurichalcite (PDF#17-0743). Only the aurichalcite phase was observed over CuZn-1. Together with the increase of peak width, the intensity of XRD reflections decreased, indicating that the crystallinity of minerals was reduced gradually by the addition of Zn^{2+}. XRD results revealed that pure malachite was exhibited over CuZn-inf; pure rosasite was formed over CuZn-4 and CuZn-3; the mixed composite of both rosasite and aurichalcite was observed over CuZn-2 while only aurichalcite could be detected over CuZn-1.
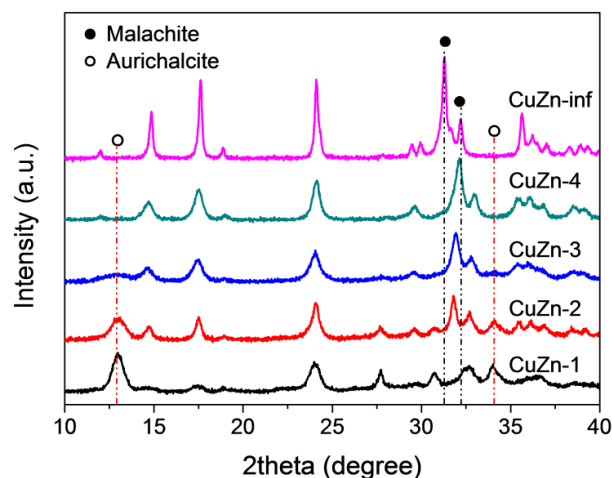

Figure 1 XRD patterns of the precursors of CuZn-x catalysts.

IR spectra visualized the structure evolutions of precursors (**Figure 2a and 2b**). The bands in the region of 400-600 cm^{-1} are attributed to Cu-O and/or Zn-O bonds.[28] With the increase of Zn^{2+} contents, these bands broadened, shifted to lower frequencies and decreased in intensity. According to Stoilova et al.[28], this could be attributed to the stronger Cu-O interactions and higher polarization ability of Zn^{2+} ions, indicating the substitution of Cu^{2+} by Zn^{2+} ions. The bands at 712 and 752 cm^{-1} are the ν_4

This journal is © The Royal Society of Chemistry [year]

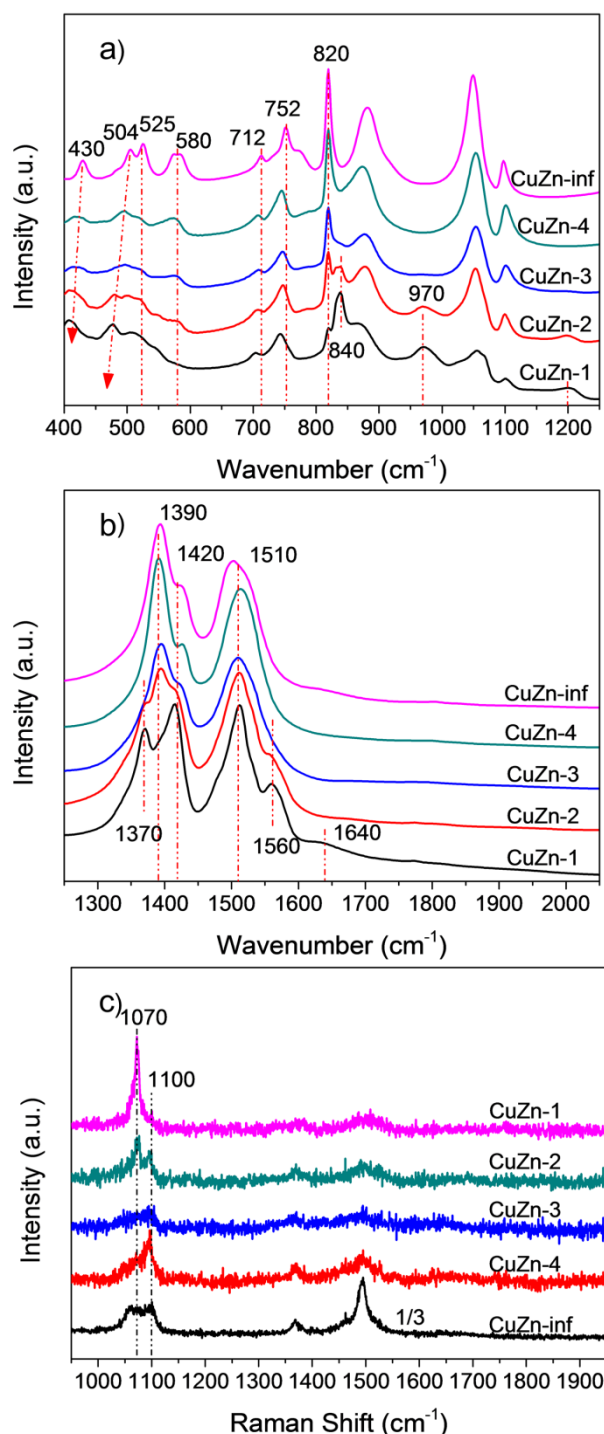*Catal. Sci. Technol.*, [year], **[vol]**, 00–00 | **3**

Figure 2 IR (a: 400-1250 cm^{-1}, b: 1250-2050 cm^{-1}) and Raman spectra (c, intensity of CuZn-inf was divided by 3 times) of the CuZn-x precursors.

asymmetric OCO bending modes[28], which shifted to lower wavenumbers when Cu^{2+} were replaced by Zn^{2+} ions. The peak at 820 cm^{-1} is the indicative of ν_2 mode of malachite and rosasite, which diminished gradually with the increase of Zn^{2+} content.[29] Furthermore, it is interesting to note that slight remnant at 820 cm^{-1} was observed over CuZn-1, indicating the existence of slight amount of rosasite over the sample which is lower than the detection limit of XRD. A new peak at 840 cm^{-1} emerged over CuZn-2 and CuZn-1 which can be attributed to ν_2 mode of

aurichalcite. The bands at 970 and 1200 cm^{-1} can also serve as the fingerprint bands of aurichalcite.[28, 29] For malachite and rosasite, bands in the range of 1300-1600 cm^{-1} are attributed to ν_4 modes of CO_3^{2-} ions (**Figure 2b**). When malachite and rosasite minerals changed into aurichalcite, the bands in this range would be complicated due to the existence of two crystallographically non-equivalent CO_3^{2-} ions bonded to different ions (Cu^{2+} and Zn^{2+}). The band at 1390 cm^{-1} disappeared while the bands at 1370 and 1560 cm^{-1} emerged with the addition of Zn^{2+} ions. The IR results confirmed the structural evolutions of precursors, as evidenced by XRD results.

Raman spectroscopy has been proven very useful for studying the minerals precursors (**Figure 2c**). The band at 1070 cm^{-1} corresponds to the CO_3^{2-} symmetric stretching mode of aurichalcite while the peak at 1100 cm^{-1} belongs to the rosasite phase.[32, 37] For CuZn-2, the overlapped peaks at 1070 and 1100 cm^{-1} were attributed to the mixed crystal phases of aurichalcite and rosasite. A different motif of CuZn-inf was observed in the range of 1050-1150 cm^{-1}, which could be ascribed to the overlapped peak of O-H out-of-plane bending mode and ν_1 CO_3^{2-} symmetric stretching mode of malachite.[33, 34] Raman results supported the observations of IR experiments.

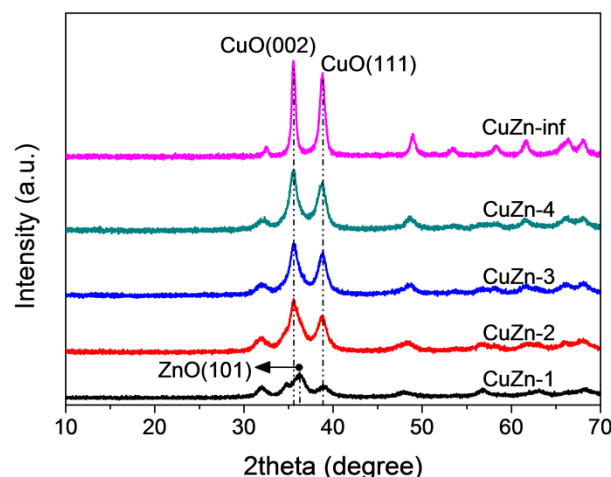**Characterizations of calcined and reduced catalysts**

Figure 3 XRD patterns of the calcined CuZn-x catalysts (CuO, PDF#45-0937; ZnO, PDF#36-1451).

Table 1 gives an overview of main physicochemical and surface properties of CuZn-x catalysts. The elemental compositions and Cu/Zn molar ratios, determined by ICP experiments, fitted well with the nominal values. CuZn-inf exposed a surface area (S$_{BET}$) of ~18 m^2/g which was approximate one-third of CuZn-x (x=1, 2, 3, 4) catalysts. The pore volume (V$_p$) of CuZn-inf was also lower than other samples. The results indicated that Zn^{2+} tuned structures of precursors and the microstructures of catalysts. The amounts of surface metallic Cu sites (S$_{Cu}$) and surface acid concentrations (S$_{acid}$) were determined by N$_2$O and NH$_3$-TPD experiments respectively. CuZn-inf showed the lowest S$_{Cu}$ and S$_{acid}$. S$_{Cu}$ increased with the decrease of Cu/Zn molar ratios and reached the maximum at Cu/Zn ratio of 2. When Cu/Zn ratio was further decreased, a decrease of S$_{Cu}$ was observed. In contrast, S$_{acid}$ increased monotonously when Cu^{2+} was substituted by Zn^{2+}, indicating that the surface acidity was mainly arisen from ZnO

4 | *Catal. Sci. Technol.*, [year], **[vol]**, 00–00

This journal is © The Royal Society of Chemistry [year]

Table 1 The main physicochemical and structural properties of CuZn-x catalysts.

Catalysts	Cu content (wt. %)[a]	Zn content (wt. %)[a]	Cu/Zn molar ratios	S_{BET} (m²/g)[b]	d_p (nm)[b]	V_p (cm³/g)[b]	d_{CuO} (nm)[c]	S_{Cu} (mmol/g$_{cat}$)[d]	S_{acid} (mmol/g$_{cat}$)[e]
CuZn-inf	79.6	–	–	18.0	20.7	0.17	11.4	0.39	3.70×10^{-4}
CuZn-4	63.8	15.9	4.1	52.4	14.6	0.27	7.4	1.55	6.20×10^{-4}
CuZn-3	60.0	19.5	3.2	56.9	12.9	0.25	7.1	2.03	1.06×10^{-3}
CuZn-2	53.7	26.3	2.1	55.7	11.5	0.24	6.2	2.12	1.16×10^{-3}
CuZn-1	40.3	39.4	1.1	55.8	13.3	0.26	6.1	1.78	1.27×10^{-3}

[a] Determined by ICP experiments. [b] Determined by N₂ adsorption experiments. [c] Calculated by CuO(111) reflection at 38.7° based on Scherrer equation. [d] amounts of surface metallic Cu sites (S_{Cu}) were determined by N₂O titration measurements. [e] surface acid concentrations (S_{acid}) were determined by NH₃-TPD measurements.
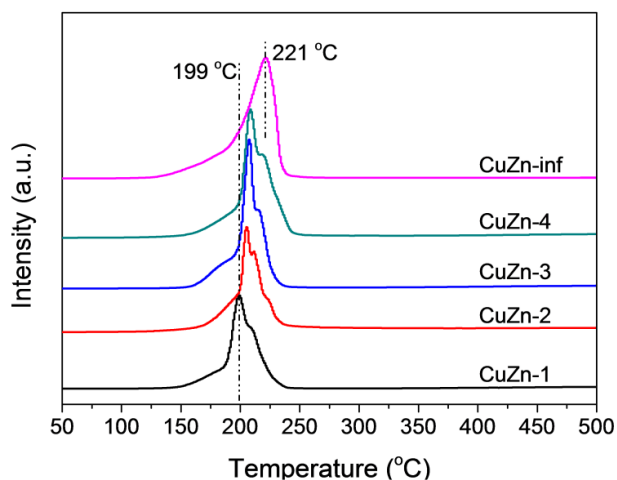
Figure 4 TPR results of the calcined CuZn-x catalysts.
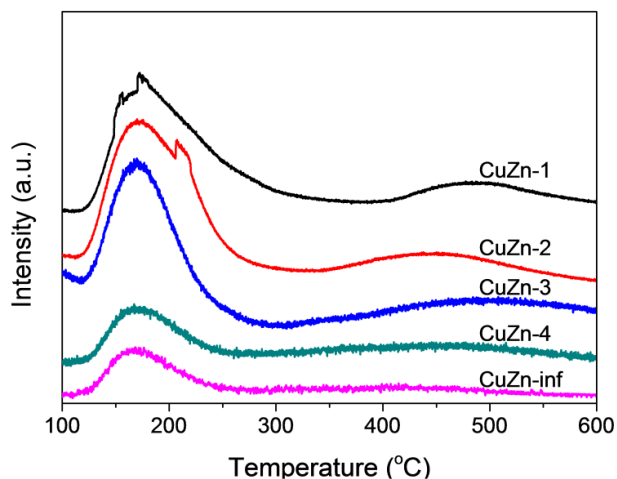
Figure 5 NH₃-TPD results of the calcined CuZn-x catalysts.

component.[38]

Calcination of the precursors resulted in the formation of oxide composites containing an intimate mixture of CuO and ZnO species. **Figure 3** shows the XRD patterns of calcined CuZn-x catalysts. The CuO reflections at 35.6° (002) and 38.7° (111) were broad over all the calcined catalysts, indicating that CuO particles over CuZn-x catalysts were small (PDF#45-0937). Moreover, the intensity of CuO peaks decreased and full widths at half maximum of peaks increased with the addition of Zn²⁺, demonstrating the decrease of CuO particle sizes and the role of Zn²⁺ for dispersing CuO species. No crystalline ZnO was detected over CuZn-x (2, 3, 4 and inf) catalysts, indicating the

high dispersion of ZnO species. Only a weak peak of ZnO at 36.3° (PDF#36-1451, crystalline size is 9.4 nm) was observed over CuZn-1. Because the diffraction of CuO(002) at 35.6° is greatly overlapped with that of ZnO(101), we therefore used the reflection of CuO(111) at 38.7° to quantitatively determine the CuO particle sizes (d_{CuO}) (**Table 1**). Mean CuO crystalline sizes of CuZn-x (x=1, 2, 3, 4) were 6.1-7.4 nm, whereas that of CuZn-inf was 11.4 nm. The above results demonstrated that minerals precursors can facilitate the high dispersions of catalyst components. To investigate the reducibility and structural evolutions of CuZn-x catalysts, TPR experiments were performed (**Figure 4**). CuZn-inf exhibited the highest reduction temperature as a result of the largest CuO crystallites and poor porous structures.[39] Concomitantly, the TPR profile of CuZn-inf was different from that of CuZn-x (x=1, 2, 3, 4) catalysts, which might be because of the absence of ZnO. The CuZn-x (x=1, 2, 3, 4) catalysts all exhibited a broad peak composed of multi-shoulders. With the increase of ZnO content, the peaks of CuZn-x catalysts migrated slightly towards the lower temperature side, of which CuZn-1 showed the lowest reduction temperature. The results fitted well with the observations of XRD results.[40] For the CuZn-x catalysts, the shoulder at higher temperature side can be attributed to the reduction of Cu²⁺ species which interacted strongly with ZnO species.[41] The TPR results revealed that the reduction behaviors can also be complicated by the interactions between CuO and ZnO.

The surface acidity of CuZn-x catalysts was determined by NH₃-TPD experiments (**Figure 5**). A main peak at 180 °C and a slight one in the range of 400-500 °C were observed for all the catalysts, which can be ascribed to the weak and strong acidic sites respectively. The amounts of surface acid sites were enhanced when Zn²⁺ content was increased. We calculated the amounts of surface acid sites (**Table 1**) and found that CuZn-1 catalyst exhibited the highest surface acid concentration (1.27×10^{-3} mmol/g$_{cat}$) while CuZn-inf only possessed slight surface acidity (3.70×10^{-4} mmol/g$_{cat}$). The reuslts indicated that the surface acidity was mainly arisen from ZnO species.[38] It should be noted that all the catalysts exhibited relatively low densities of surface acidity (about 3 orders lower than S_{Cu}), mainly due to the fact that ZnO was an oxide with low surface acidity. The moderate surface acid sites would facilitate the tunable production of DHMF and DMF at different conditions, which would be discussed in the following parts.

Figure 6 illustrated the correlations between Cu contents, mineral structures and the main structural and surface properties of CuZn-x catalysts. When Cu²⁺ ions were replaced by Zn²⁺ ions, the precursor structures evolved from malachite to rosasite, and

This journal is © The Royal Society of Chemistry [year]

Catal. Sci. Technol., [year], **[vol]**, 00–00 | **5**

then changed to the mixture of rosasite and aurichalcite phases, which led to the different properties of resulted catalysts. As shown in **Figure 6a**, addition of Zn^{2+} ions increased the S_{BET} of calcined catalysts for ~3 times and decreased the mean CuO particle size for approximate 0.5 times. Cu dispersion increased with the decrease of Cu content, which resulted in a comprehensive volcano trend of surface metallic Cu concentrations (**Figure 6b**). CuZn-2 exposed the maximum amount of surface Cu sites. In contrast, the amount of surface acid sites increased with the decrease of Cu content, indicating that ZnO species may be responsible for the surface acidity.
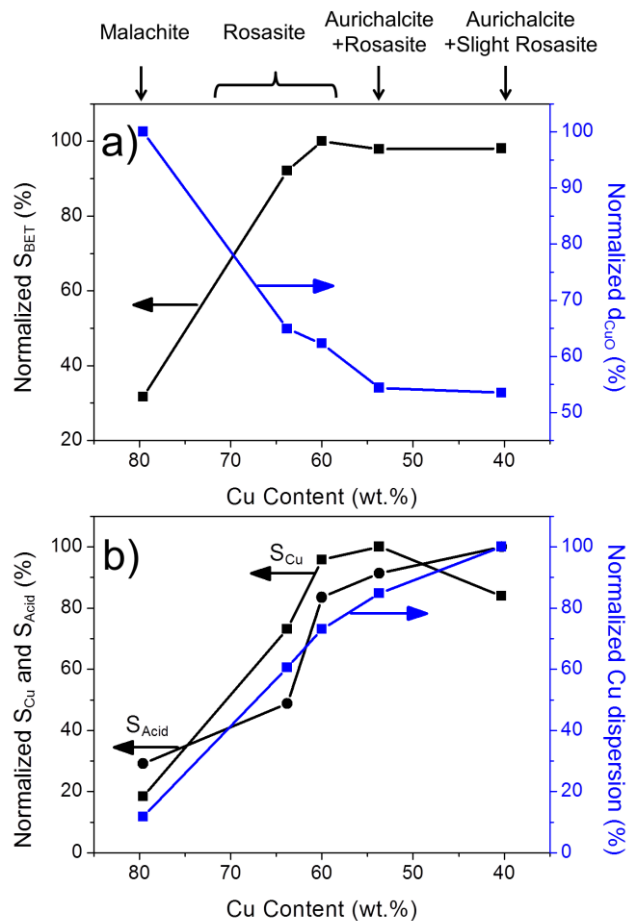

Figure 6 Correlations between main physic-chemical properties and Cu contents of CuZn-x catalysts (Normalized: the highest is 100%).

Performance of CuZn-x catalysts for DHMF synthesis

The selective hydrogenation of HMF to DHMF over CuZn-x catalysts was conducted at 100 °C and 1.5 MPa for 1 h. The performance of CuZn-x catalysts was screened (**Table 2**). The commercial Raney metal (Ni, Co and Cu) catalysts were also employed as references. A low HMF conversion of ~16.3% was obtained over CuZn-inf. With the decrease of Cu/Zn ratios, HMF conversion firstly increased, reached the maximum of 83.5% over CuZn-2 catalyst and then decreased, while DHMF selectivity was almost constant around 99%. The activity follows the similar trend of surface metallic Cu concentrations (**Figure S1**). Interestingly, CuZn-1 and CuZn-3 possessed different surface metallic Cu concentrations, but showed similar activity towards

HMF hydrogenation to DHMF. According to Morrison et al.[42], acid can help the activation of carbonyl groups and thus facilitate the reactivity. The similar reactivity of CuZn-1 and CuZn-3 can be attributed to the synergy between surface metallic Cu sites and acid sites. The results revealed that ZnO not only dispersed Cu sites, but also provided some acid sites for promoting HMF hydrogenation. It should be noted that bare ZnO without metallic Cu sites can hardly catalyze HMF hydrogenation in our cases, as evidenced by model tests (**Table S1**).

Table 2 HMF hydrogenation over CuZn-x catalysts and commercial Raney metals at 100 °C.[a]

Catalysts	Conv. (%)	Sel. (%)		
		DHMF	DHMTHF	Others[b]
CuZn-inf	16.3	98.1	0	1.9
CuZn-4	34.1	97.9	0	2.1
CuZn-3	75.4	98.9	0	1.1
CuZn-2	83.5	99.1	0	0.9
CuZn-1	75.3	99.2	0	0.8
Raney Cu	60.0	98.9	0	1.1
Raney Co	63.9	97.2	2.7	1.2
Raney Ni	73.1	69.5	20.1	10.4

[a] Conditions: 1.5 MPa, 1 h, catalyst 0.5 g, HMF 1.5 g. [b] Others mainly contain DMF and 5-methylfurfuryl alcohol (MFA).
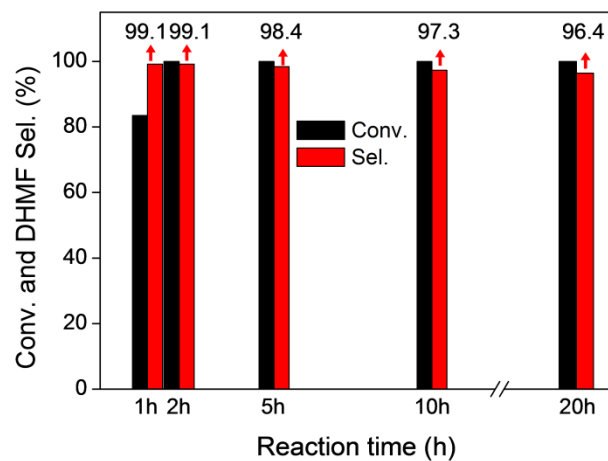

Figure 7 Time course of catalytic performance of CuZn-2 catalyst at 100 °C (1.5 MPa H_2, HMF 1.5 g, catalyst 0.5 g).

The effectiveness of the CuZn-2 catalyst was also compared with commercial Raney Cu, Co and Ni catalysts at the same reaction conditions. Among the Raney metals, Raney Ni exhibited the highest activity with a HMF conversion of 73.1%, which was still lower than CuZn-2 catalyst. The superior performance of CuZn-2 catalyst indicated that mineral precursors could facilitate the formation of highly dispersed metal sites and high catalytic activity. Moreover, the DHMF selectivity of Raney Ni was much lower than CuZn-2 catalyst, mainly due to the formation of DHMTHF. DHMTHF is formed by ring hydrogenation of DHMF. Thus, the formation of DHMTHF over Raney Ni indicates the relatively strong C=C hydrogenation ability of Ni, which is detrimental to DHMF synthesis.[17] In contrast, CuZn-x and Raney Cu catalysts exhibited high

6 | *Catal. Sci. Technol.*, [year], **[vol]**, 00–00

This journal is © The Royal Society of Chemistry [year]

selectivity of DHMF, indicating that the catalysts have high reactivity of C=O bonds while have relatively low reactivity toward C=C hydrogenation. Extensive studies regarding the configuration for adsorbed aldehydes have been conducted over Cu surface. The $\eta^1(O)$ configuration is known to be formed[43, 44]; and thus Cu-based catalysts could exhibit high selectivity to C=O hydrogenation. The above results confirmed that mineral-derived Cu-based catalysts are good candidates for selective hydrogenation of HMF to DHMF.

Time course of CuZn-2 catalyst at 100 °C and 1.5 MPa were studied to achieve the highest reactivity and DHMF yield. As plotted in **Figure 7**, HMF conversion increased from 83.5% to 100% upon increasing the reaction time from 1 h to 2 h, while the selectivity was almost unchangeable. Further increase of reaction time (up to 20 h) had little effect on the DHMF selectivity. The performance of CuZn-x catalysts at 100 °C for 20 h were also compared (**Figure S2**), which all exhibited high DHMF yields. Very slight amount of hydrogenolysis and ring-saturation byproducts (MFA, DMF and DHMTHF) were detected under the conditions. The results revealed the high selectivity of Cu-ZnO catalysts towards synthesis of DHMF at 100 °C.

Selective conversion of HMF to DMF

Selective hydrogenation of HMF to DMF contains the hydrogenation of C=O bond and hydrogenolysis of C-O bonds, which is a more challenging reaction than DHMF synthesis. DHMF is the main intermediate for DMF over Cu catalysts while 2,5-dimethyltetrahydrofuran (DMTHF) is the over-hydrogenated product.[20]

Table 3 Influence of reaction temperature for HMF hydrogenation over CuZn-2 catalyst.

T/°C	Conv. (%)	Sel. (%)				
		DHMF	MFA	DMF	DMTHF	Others
80	53.7	99.5	0	0	0	0.5
100	83.5	99.1	0.2	0	0	0.7
140	97.5	94.4	3.6	1.8	0	0.2
180	100	50.0	20.9	27.4	1.6	0.1
220	100	33.1	24.1	40.6	1.9	0.3

^{a} Conditions: 1.5 MPa, 1 h, catalyst 0.5 g, HMF 1.5 g.

DHMF had been already obtained effectively over CuZn-2 catalyst at 100 °C. The hydrogenolysis of C-O bonds would be significantly promoted by elevation of reaction temperatures, as reported in previous works.[17, 20] The effect of reaction temperature on the performance of CuZn-2 catalyst was therefore studied (**Table 3**). At 80 °C, 53.7% of HMF was converted into DHMF with ~99.5% selectivity. The conversion increased to 83.5% when the temperature was elevated to 100 °C and the DHMF selectivity was maintained around 99%. With further increase of reaction temperature to 140 °C, HMF was almost totally converted while DHMF selectivity dropped due to the formation of MFA and DMF. Further increase of reaction temperature tuned the product distribution dramatically. DHMF selectivity decreased, whereas MFA and DMF selectivity increased monotonously. The best DMF selectivity of ~40.6% was obtained at 220 °C. Moreover, DHMF and MFA were obtained with a total

yield of 57.2%, which could be converted to DMF by hydrogenolysis of side –CH$_2$OH group.[17] In all, the results showed that high reaction temperature would promote C-O hydrogenolysis reactions, while the DMF yield could be further improved. Therefore, 220 °C was chosen to further optimize the DMF selectivity. The above results facilitated the potential tunable synthesis of DMF and DHMF over Cu-ZnO catalysts.
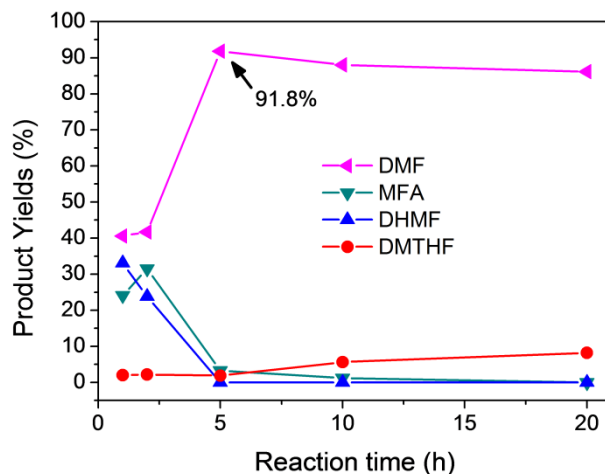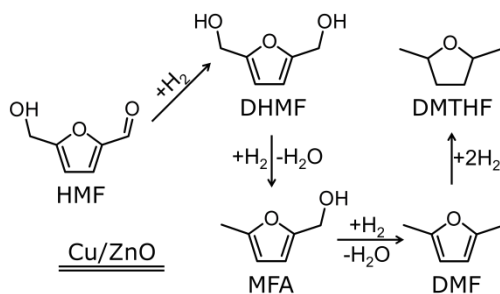

Figure 8 Time course of catalytic performance of CuZn-2 catalyst at 220 °C (1.5 MPa H$_2$, HMF 1.5 g, catalyst 0.5g).

Scheme 3 Reaction pathway of HMF hydrogenation under the conditions.

Figure 8 showed the time course of catalytic performance of CuZn-2 catalyst at 220 °C and 1.5 MPa. Upon increase of the reaction time from 1 h to 2 h, the DMF yield did not change dramatically, whereas DHMF yield decreased with the elevation of MFA yield. After 5 h reaction time, DHMF and MFA were almost totally consumed, giving rise to a high DMF yield of 91.8%, indicating that C-O hydrogenolysis was promoted. Upon the further increase in reaction time, DMF selectivity decreased slightly due to the formation of DMTHF. Nevertheless, DMF selectivity maintained at a high level within our reaction conditions.

The above results revealed a reaction pathway for HMF hydrogenation under the reaction conditions. HMF was initially hydrogenated into DHMF (**Figure 7**). Upon increasing the reaction temperature, the generated DHMF was converted whereas MFA, DMF and very slight amount of DMTHF were formed (**Table 3**). When the reaction time was increased, DHMF was continuously converted (**Figure 8**). In contrast, MFA was firstly formed and then converted, whereas DMF was formed substantially. The yield of DMTHF increased slightly when the reaction time was increased. The reaction pathway was

summarized in **Scheme 3**.

The above results demonstrate a tunable and highly selective conversion of HMF to DHMF or DMF using a binary minerals-derived Cu-ZnO catalyst at different conditions (**Scheme 1**), confirming the potential of non-noble Cu catalysts for selective hydrogenation of HMF. Key to our success is the highly dispersed active sites, well-controlled surface acidity and suitable reaction conditions.
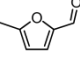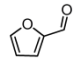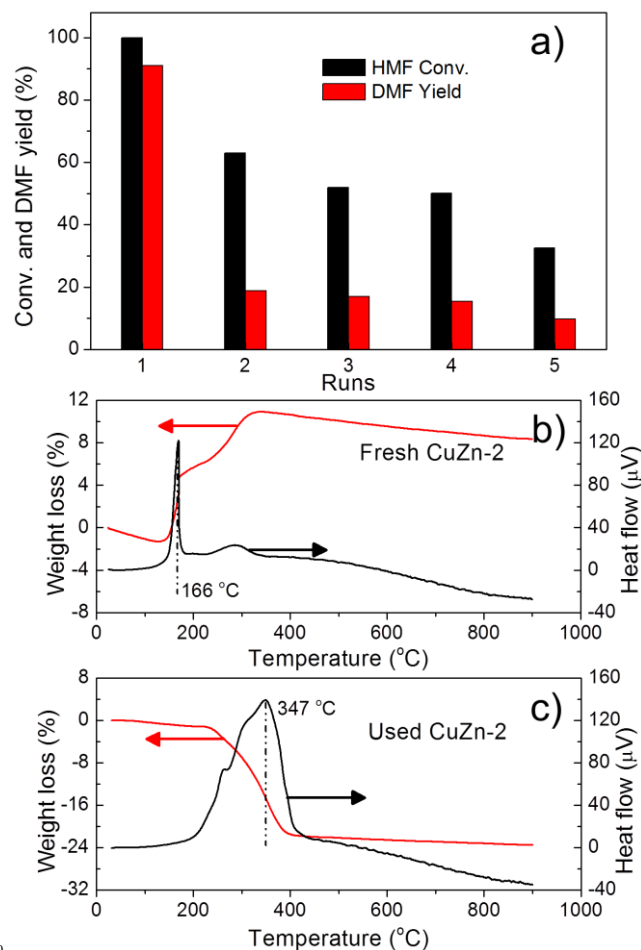
Catalyst stability

Figure 9 (a) Reusability of CuZn-2 catalyst for DMF synthesis from HMF hydrogenation (Conditions: 220 °C, 1.5 MPa, 5 h, HMF 1.5 g, catalyst 0.5 g, 1,4-dioxane 35 ml). (b) Thermo-gravity (TG) spectra of fresh reduced CuZn-2 catalyst. (c) TG spectra of used CuZn-2 catalyst.

HMF hydrogenation to DMF was chosen to further investigate the reusability of CuZn-2 catalyst due to the relatively severe condition (220 °C). A sharp decrease of HMF conversion and DMF selectivity was observed (**Figure 9a**), indicating that the catalyst deactivated during the tests. Thermo-gravity (TG) experiments of fresh reduced and used CuZn-2 catalysts were performed to examine the deposition of carbonaceous species (**Figure 9b** and **9c**). The weight of fresh reduced CuZn-2 increased, which could be ascribed to the oxidation of Cu. In contrast, the dramatic weight loss of used CuZn-2 accompanied by a sharp exothermic peak revealed the oxidization of carbonaceous species.[18] The carbonaceous species can strongly adsorb on the catalyst and hinder the activity.[19] XRD patterns

revealed that Cu particles were not evidently grown after 5 runs (**Figure S3**). Besides, the recovery processes (e.g., washing) would inevitably cause weight loss of catalyst. The results suggested that deactivation of CuZn-2 was mainly resulted from deposition of carbonaceous species, which was consistent with previous reports.[14, 18] The slight Cu particle growth and weight loss of catalyst may also cause the loss of reactivity to some extent. The deposited carbonaceous species can be removed by re-calcination and re-reduction procedures.[14, 45] Besides, design of efficient catalyst that can catalyze HMF hydrogenolysis at low temperatures can benefit the stability due to the minimization of humins formations.

Applications in conversion of bio-derived molecules

Table 4 Applications of CuZn-2 catalyst in conversion of furanic compounds.

Feedstock	Conditions[a]	Conv. (%)	Sel. (%)	
(5-methylfurfural)	100 °C, 2 h	100	(MFA)	99.2
	220 °C, 10 h	100	(DMF)	91.6
(furfural)	100 °C, 2 h	100	(furfuryl alcohol)	98.9
	220 °C, 10 h	100	(2-methylfuran)	94.5

[a] 1.5 MPa, catalyst 0.5 g, feedstock 1.5 g.

The CuZn-2 catalyst was further extended to selective hydrogenation of other bio-derived furan molecules (5-methylfurfural and furfural). As shown in **Table 4**, MFA and DMF were obtained with high yields of 99.2% and 91.6% respectively at different reaction conditions, when 5-methylfurfural was employed as the reactant. For selective hydrogenation of furfural, high yields of furfuryl alcohol (98.9%) and 2-methylfuran (94.5%) were also achieved through tuning reaction conditions. These results further demonstrated the great flexibility of mineral-based Cu-ZnO catalysts for efficiently and selectively converting bio-derived molecules. Further improvement and rational design of mineral-derived Cu catalysts are in progress.

Conclusions

The non-noble minerals-derived (malachite, rosasite and aurichalcite) Cu-ZnO catalysts prepared by simple controlled co-precipitation method have been demonstrated to have high reactivity and selectivity for conversion of HMF to either DHMF (~99.1% yield) or DMF (~91.8% yield). The tunable synthesis of both products was obtained by simply tuning the reaction temperature and reaction time. The structural evolutions of minerals and structure-performance relationships were elucidated by various characterizations on composition, structural and surface properties and catalyst tests. The Cu-ZnO catalyst derived from the mixture of rosasite and aurichalcite (CuZn-2) was found to possess the highest reactivity, which is due to the highest surface Cu concentration, proper acidity and good microstructures. The results here are expected to be useful for further rational design of earth-abundant Cu catalysts. The catalyst was also extended to selective hydrogenation of other bio-derived molecules (furfural and 5-methylfurfural) to valuable

products, demonstrating the flexibility of Cu catalyst for biomass conversions.

Notes and references

[a] *State Key Laboratory of Coal Conversion, Institute of Coal Chemistry,*
5 *Chinese Academy of Sciences, Taiyuan 030001, PR China. Fax: +86 351 7560668; Tel: +86 351 7117097; E-mail: zhuyulei@sxicc.ac.cn (Y. Zhu).*
[b] *University of Chinese Academy of Sciences, Beijing 100049, PR China.*
[c] *Synfuels China Co. Ltd, Beijing, 101407, PR China.*

10 † Electronic Supplementary Information (ESI) available: Table S1 and Figure S1-S3. See DOI: 10.1039/b000000x/

‡ The authors contribute equally.

1. R. J. van Putten, J. C. van der Waal, E. de Jong, C. B. Rasrendra, H. J. Heeres and J. G. de Vries, *Chem. Rev.*, 2013, **113**, 1499-1597.
20 2. J. N. Chheda, G. W. Huber and J. A. Dumesic, *Angew. Chem. Int. Ed.*, 2007, **46**, 7164-7183.
3. C. Zeng, H. Seino, J. Ren, K. Hatanaka and N. Yoshie, *Polymer*, 2013, **54**, 5351-5357.
4. C. Zeng, H. Seino, J. Ren, K. Hatanaka and N. Yoshie, *Macromolecules*, 2013, **46**, 1794-1802.
25 5. C. Zeng, H. Seino, J. Ren and N. Yoshie, *ACS Appl. Mater. Interfaces*, 2014, **6**, 2753-2758.
6. M. Chatterjee, T. Ishizaka and H. Kawanami, *Green Chem.*, 2014, **16**, 4734-4739.
30 7. Y. Roman-Leshkov, C. J. Barrett, Z. Y. Liu and J. A. Dumesic, *Nature*, 2007, **447**, 982-985.
8. P. T. Do, J. R. McAtee, D. A. Watson and R. F. Lobo, *ACS Catal.*, 2013, **3**, 41-46.
9. Y.-P. Li, M. Head-Gordon and A. T. Bell, *J. Phys. Chem. C*, 2014, 35 **118**, 22090-22095.
10. R. Alamillo, M. Tucker, M. Chia, Y. Pagan-Torres and J. Dumesic, *Green Chem.*, 2012, **14**, 1413-1419.
11. J. Ohyama, A. Esaki, Y. Yamamoto, S. Arai and A. Satsuma, *RSC Adv.*, 2013, **3**, 1033-1036.
40 12. J. Mitra, X. Zhou and T. Rauchfuss, *Green Chem.*, 2015, **17**, 307-313.
13. M. Tamura, K. Tokonami, Y. Nakagawa and K. Tomishige, *Chem. Commun.*, 2013, **49**, 7034-7036.
14. J. Jae, W. Zheng, R. F. Lobo and D. G. Vlachos, *ChemSusChem*, 2013, **6**, 1158-1162.
45 15. Y. Zu, P. Yang, J. Wang, X. Liu, J. Ren, G. Lu and Y. Wang, *Appl. Catal. B: Environ.*, 2014, **146**, 244-248.
16. G. H. Wang, J. Hilgert, F. H. Richter, F. Wang, H. J. Bongard, B. Spliethoff, C. Weidenthaler and F. Schuth, *Nat. Mater.*, 2014, **13**, 293-300.
50 17. X. Kong, Y. Zhu, H. Zheng, F. Dong, Y. Zhu and Y.-W. Li, *RSC Adv.*, 2014, **4**, 60467-60472.
18. X. Kong, R. Zheng, Y. Zhu, G. Ding, Y. Zhu and Y.-W. Li, *Green Chem.*, 2015, **17**, 2504-2514.
19. Y. B. Huang, M. Y. Chen, L. Yan, Q. X. Guo and Y. Fu, 55 *ChemSusChem*, 2014, **7**, 1068-1072.
20. A. J. Kumalaputri, G. Bottari, P. M. Erne, H. J. Heeres and K. Barta, *ChemSusChem*, 2014, **7**, 2266-2275.
21. T. S. Hansen, K. Barta, P. T. Anastas, P. C. Ford and A. Riisager, *Green Chem.*, 2012, **14**, 2457.
60 22. Y. Nakagawa, K. Takada, M. Tamura and K. Tomishige, *ACS Catal.*, 2014, **4**, 2718-2726.
23. E. R. Sacia, M. Balakrishnan and A. T. Bell, *J. Catal.*, 2014, **313**, 70-79.
24. Y. Zhu, X. Kong, D.-B. Cao, J. Cui, Y. Zhu and Y.-W. Li, *ACS* 65 *Catal.*, 2014, **4**, 3675-3681.
25. E. S. Vasiliadou, T. M. Eggenhuisen, P. Munnik, P. E. de Jongh, K. P. de Jong and A. A. Lemonidou, *Appl. Catal. B: Environ.*, 2014, **145**, 108-119.

26. H. Tan, M. N. Hedhill, Y. Wang, J. Zhang, K. Li, S. Sioud, Z. A. Al-70 Talla, M. H. Amad, T. Zhan, O. E. Tall and Y. Han, *Catal. Sci. Technol.*, 2013, **3**, 3360.
27. B. Bems, M. Schur, A. Dassenoy, H. Junkes, D. Herein and R. Schlögl, *Chem. Eur. J.*, 2003, **9**, 2039-2052.
28. D. Stoilova, V. Koleva and V. Vassileva, *Spectrochim. Acta A*, 2002, 75 **58**, 2051-2059.
29. M. Behrens, F. Girgsdies, A. Trunschke and R. Schlögl, *Eur. J. Inorg. Chem.*, 2009, **2009**, 1347-1357.
30. M. Behrens, *J. Catal.*, 2009, **267**, 24-29.
31. M. Behrens and F. Girgsdies, *Z. Anorg. Allg. Chem.*, 2010, **636**, 919-80 927.
32. R. L. Frost, M. C. Hales and B. Jagannadha Reddy, *Polyhedron*, 2007, **26**, 3291-3300.
33. R. L. Frost, D. L. Wain, W. N. Martens and B. J. Reddy, *Spectrochim. Acta A*, 2007, **66**, 1068-1074.
85 34. R. L. Frost, *J. Raman Spectrosc.*, 2006, **37**, 910-921.
35. R. L. Frost, B. J. Reddy, D. L. Wain and W. N. Martens, *Spectrochim. Acta A*, 2007, **66**, 1075-1081.
36. S. Zander, E. L. Kunkes, M. E. Schuster, J. Schumann, G. Weinberg, D. Teschner, N. Jacobsen, R. Schlögl and M. Behrens, *Angew. Chem.* 90 *Int. Ed.*, 2013, **52**, 6536-6540.
37. R. L. Frost, W. N. Martens, L. Rintoul, E. Mahmutagic and J. T. Kloprogge, *J. Raman Spectrosc.*, 2002, **33**, 252-259.
38. Y. Zhu, X. Kong, X. Li, G. Ding, Y. Zhu and Y.-W. Li, *ACS Catal.*, 2014, **4**, 3612-3620.
95 39. Y. Zhu, Y. Zhu, G. Ding, S. Zhu, H. Zheng and Y. Li, *Appl. Catal. A: Gen.*, 2013, **468**, 296-304.
40. L. Shi, C. Zeng, Y. Jin, T. Wang and N. Tsubaki, *Catal. Sci. Technol.*, 2012, **2**, 2569.
41. J. Agrell, K. Hasselbo, K. Jansson, S. G. Järås and M. Boutonnet, 100 *Appl. Catal. A: Gen.*, 2001, **211**, 239-250.
42. R. Morrison and R. Boyd, *Organic Chemistry, 6th*, Englewood Cliffs, NJ: Prentice Hall, 1992.
43. S. Sitthisa, T. Sooknoi, Y. Ma, P. B. Balbuena and D. E. Resasco, *J. Catal.*, 2011, **277**, 1-13.
105 44. Y. Nakagawa, H. Nakazawa, H. Watanabe and K. Tomishige, *ChemCatChem*, 2012, **4**, 1791-1797.
45. B. J. O'Neill, D. H. Jackson, A. J. Crisci, C. A. Farberow, F. Shi, A. C. Alba-Rubio, J. Lu, P. J. Dietrich, X. Gu, C. L. Marshall, P. C. Stair, J. W. Elam, J. T. Miller, F. H. Ribeiro, P. M. Voyles, J. Greeley, M. 110 Mavrikakis, S. L. Scott, T. F. Kuech and J. A. Dumesic, *Angew. Chem. Int. Ed.*, 2013, **52**, 13808-13812.